ARTICLE
Journal of Cellular Biochemistry 113:2136–2146 (2012)

Journal of Cellular Biochemistry

# Phenotypic Characterization of Transgenic Mice Harboring Nf1$^{+/-}$ or Nf1$^{-/-}$ Osteoclasts in Otherwise Nf1$^{+/+}$ Background

Maria H. Alanne,[1] Elina Siljamäki,[2,3] Sirkku Peltonen,[2,4] Kalervo Väänänen,[1] Jolene J. Windle,[5] Luis F. Parada,[6] Jorma A. Määttä,[1,7] and Juha Peltonen[1*]

[1]*Department of Cell Biology and Anatomy, University of Turku, Turku, Finland*
[2]*Department of Dermatology, University of Turku, Turku, Finland*
[3]*MediCity Research Laboratory, University of Turku, Turku, Finland*
[4]*Department of Dermatology, Turku University Hospital, Turku, Finland*
[5]*Department of Human and Molecular Genetics, Virginia Commonwealth University, Richmond, Virginia*
[6]*Department of Developmental Biology and Kent Waldrep Foundation Center for Basic Research on Nerve Growth and Regeneration, University of Texas Southwestern Medical Center, Dallas, Texas 75390*
[7]*Turku Center for Disease Modeling, University of Turku, Turku, Finland*

## ABSTRACT

Skeletal abnormalities in neurofibromatosis type 1 syndrome (NF1) are observed in ~50% of patients. Here, we describe the phenotype of Nf1$_{Ocl}$ mouse model with Nf1-deficient osteoclasts. Nf1$_{Ocl}$ mice with Nf1$^{+/-}$ or Nf1$^{-/-}$ osteoclasts in otherwise Nf1$^{+/+}$ background were successfully generated by mating parental Nf1flox/flox and TRAP-Cre mice. Contrary to our original hypothesis, osteoporotic or fragile bone phenotype was not observed. The μCT analysis revealed that tibial bone marrow cavity, trabecular tissue volume, and the perimeter of cortical bone were smaller in Nf1$^{-/-}_{Ocl}$ mice compared to Nf1$^{+/+}_{Ocl}$ control mice. Nf1$^{-/-}_{Ocl}$ mice also a displayed narrowed growth plate in the proximal tibia. In vitro analysis showed increased bone resorption capacity and cytoskeletal changes including irregular cell shape and abnormal actin ring formation in Nf1$^{-/-}$ osteoclasts. Surprisingly, the size of spleen in Nf1$^{-/-}_{Ocl}$ mice was two times larger than in controls and histomorphometric analysis showed splenic megakaryocytosis. In summary, Nf1Ocl mouse model presented with a mild but specific bone phenotype. This study shows that NF1-deficiency in osteoclasts may have a role in the development of NF1-related skeletal abnormalities, but Nf1-deficiency in osteoclasts in Nf1$^{+/+}$ background is not sufficient to induce skeletal abnormalities analogous to those observed in patients with NF1. J. Cell. Biochem. 113: 2136–2146, 2012. © 2012 Wiley Periodicals, Inc.

**KEY WORDS:** BONE DYNAMICS; OSTEOCLASTOGENESIS; RAS-ERK PATHWAY; CTX; ACTIN RING

Neurofibromatosis type 1 (NF1) syndrome is an autosomal dominant disorder which results from mutations in the NF1 gene [Riccardi and Eichner, 1986]. The human NF1 tumor suppressor gene is located on the long arm of chromosome 17 and the mouse Nf1 gene is located on chromosome 11[Buchberg et al., 1990]. The NF1 gene product, neurofibromin, accelerates the hydrolysis of active Ras-GTP to inactive Ras-GDP thus regulating cell proliferation and differentiation [Xu et al., 1990]. NF1 is associated with a wide range of manifestations with complex pathoethiology including pigmented café-au-lait spots of the skin, axillary and

Abbreviations used: NF1, neurofibromatosis type 1; Nf1, mouse neurofibromatosis type 1 gene; RANKL, receptor activator of nuclear factor κB ligand; M-CSF, magrophage colony-stimulating factor; Nf1$_{Ob}$, Nf1flox × 2.3 kb α1 (I) collagen cre; Nf1$^{Prx}$, Nf1flox × Prx1Cre positive; Nf1$^{flox/-}$; Col2.3Cre+, Nf1flox/- × Col2.3Cre+; Nf1$^{-/-}_{Col2}$, Nf1flox/flox × Col2α1-Cre; Nf1$_{Ocl}$, Nf1 flox/flox × TRAP-Cre mice; TRACP (earlier TRAP), tartrate resistant acid phosphatase; MK, megakaryocyte; CTX, C-terminal telopeptide of type I collagen; WGA, wheat germ agglutinin; μCT, microcomputer tomography.

The authors declare that they have no competing interests.

Grant sponsor: Academy of Finland; Grant number: 127080.

*Correspondence to: Juha Peltonen, Department of Cell Biology and Anatomy, University of Turku, Kiinamyllynkatu 10, 20520 Turku, Finland. E-mail: juhpel@utu.fi

Manuscript Received: 22 July 2011; Manuscript Accepted: 25 January 2012

Accepted manuscript online in Wiley Online Library (wileyonlinelibrary.com): 3 February 2012

DOI 10.1002/jcb.24088 • © 2012 Wiley Periodicals, Inc.

inguinal freckling, multiple cutaneous neurofibromas, Lisch nodules of the iris, learning disabilities, and various skeletal manifestations [Riccardi and Eichner, 1986; Jouhilahti et al., 2011]. Approximately 50% of NF1 patients have some form of a detectable skeletal manifestation [Elefteriou et al., 2009], which can be classified to generalized and focal abnormalities. The most common findings, osteopenia/osteoporosis, macrocephaly, mild scoliosis, and short stature are characterized as mild symptoms. Rare focal abnormalities such as congenital pseudarthrosis of long bones are often difficult to treat and dystrophic scoliosis is associated with significant morbidity [Elefteriou et al., 2009].

Bone dynamics includes continuous bone resorption by osteoclasts and synthesis of new bone tissue by osteoblasts secreting of receptor activator of nuclear factor κB ligand (RANKL), macrophage colony-stimulating factor (M-CSF) and osteoprotegerin (OPG) [Rodan and Martin, 1981; Biskobing et al., 1995; Simonet et al., 1997]. These catabolic and anabolic processes are linked through cellular interactions. RANKL and M-CSF promote osteoclast precursor cells to differentiate and fuse to multinuclear osteoclasts, while OPG, which is a decoy receptor for RANKL, down regulates osteoclastogenesis [Yasuda et al., 1998]. In general, osteoclasts have six key signaling pathways via RANKL receptor: extracellular signal-regulated kinase (ERK), nuclear factor of activated T-cell (NFAT), nuclear factor kappa B (NF-κB), Jun N-terminal kinase (JNK), Akt and p38 [Feng, 2005]. NF1-deficiency has been linked to alterations in Ras/Erk and Akt/mTOR signaling pathways [Elefteriou et al., 2006; Yang et al., 2006; Kolanczyk et al., 2007; Ma et al., 2012]. NF1-related susceptibility to osteoporosis suggests that the bone dynamics is imbalanced in this condition. This is also supported by the fact that NF1-deficient osteoclast cultures display increased bone resorption capacity compared to healthy control osteoclasts in man and mice [Yang et al., 2006; Heervä et al., 2010].

Neurofibromin is expressed in osteoblasts, osteocytes, osteoclasts, and chondrocytes in man and mouse [Kuorilehto et al., 2006; Yang et al., 2006; Leskelä et al., 2009]. Inactivation of the NF1 gene facilitates hyperactivation of Ras-Erk pathways at least in osteoblasts, chondrocytes and osteoclasts in vitro [Elefteriou et al., 2006; Yang et al., 2006; Kolanczyk et al., 2007]. In order to model human skeletal manifestations, different Nf1-deficient mouse strains have been studied [Yu et al., 2005; Elefteriou et al., 2006; Kolanczyk et al., 2007; Wang et al., 2011; Zhang et al., 2011]. Since inactivation of both Nf1 alleles in all cell types leads to the death of embryos on E12.5-14.5 [Brannan et al., 1994], and no marked bone abnormalities in $Nf1^{+/-}$ mice have been detected [Jacks et al., 1994; Yu et al., 2005], bone cell specific Nf1 knockout mice models with targeted inactivation of Nf1 gene in particular cell types have been generated. To elucidate the role of Nf1-deficiency in osteoblasts and their precursors, four Nf1 conditional knock out mouse models have been established [Elefteriou et al., 2006; Kolanczyk et al., 2007; Wang et al., 2011; Zhang et al., 2011]. In the $Nf1_{ob}$ mouse model, collagen type I promoter-induced Cre expression leads to inactivation of the Nf1 gene in osteoblasts. This mouse model displayed decreased mineralization and accelerated bone resorption due to activated osteoclastogenesis [Elefteriou et al., 2006]. In the $Nf1^{Prx}$ mouse model, inactivation of Nf1 gene in undifferentiated mesenchymal cells leads to several bone phenotypes with growth retardation, stunted limbs, bowing tibia, increased bone porosity and decreased calcium content [Kolanczyk et al., 2007], and skeletal muscle dystrophy [Kossler et al., 2011]. The results of another collagen type I specific, $Nf1^{flox/-}$; $Col2.3Cre^{+}$ mouse strain showed several vertebral defects such as short and lowered mechanical strength in vertebral segments and enlargement of the intervertebral canal [Zhang et al., 2011]. In the $Nf1^{-/-}_{Col2}$ mouse model, collagen type II promoter induced inactivation of Nf1 gene in osteochondroprogenitor cells and their progeny, including chondrocytes and osteoblasts. The results showed strong bone phenotype including vertebral scoliosis, scull defects, long bone dysplasia, and chest wall defects as well as osteoporotic bone [Wang et al., 2011]. These findings resemble skeletal manifestations seen in NF1 patients. In summary, these mouse models resulted in Nf1-deficiency in immature mesenchymal stem cells or differentiated cells such as osteoblasts and/or chondrocytes.

In this study, we designed a mouse model where inactivation of the Nf1 gene was directed to bone resorbing osteoclasts. The knockout model was generated by mating Nf1flox/flox and TRAP-Cre mouse strains. The mating yielded transgenic mice with $Nf1^{+/-}$ or $Nf1^{-/-}$ osteoclasts in otherwise $Nf1^{+/+}$ background.

## MATERIALS AND METHODS

### GENERATION OF TRANSGENIC MICE AND GENOTYPING

Nf1flox/flox mouse strain carrying LoxP recombination recognition sequences flanking exons 31 and 32 of the Nf1 gene has been generated in the laboratory of Dr. Luis Parada (University of Texas Southwestern Medical Center) [Zhu et al., 2001]. TRAP-Cre mouse strain [Dossa et al., 2010] has been generated by Dr Jolene Windle (Virginia Commonwealth University, Richmond, VA). Mating the Nf1flox/flox and TRAP-Cre mice produced the $Nf1_{Ocl}$ mouse strain. For genotyping, DNA was isolated from ear marks with DNeasy® Blood & Tissue Kit (Qiagen, Hilden, Germany) by protocol provided by the manufacturer. The PCR was performed using primers described previously [Zhu et al., 2001]. PCR with primer pair P1–P4 detected the Nf1flox allele and LoxP produced a 350-bp band, PCR with primer pair P1–P3 showed band from the WT allele (480 bp) and third primer pair P1–P2 detected completion of Cre-mediated recombination. PCR was performed under the following conditions: 200 μM of dNTPs, 1× Phusion HF™ buffer (Finnzymes, Espoo, Finland), 0.5 μM of primers, and 0.02 U/μl Phusion™ Hot Start High-Fidelity DNA Polymerase (Finnzymes); in conditions: denaturation at 98°C for 2 min; 35 cycles with denaturation at 98°C for 30 s; annealing at 60°C for 30 s; and extension at 72°C for 30 s; followed by 72°C for 5 min. The sequences for primers (5′ to 3′) are: P1, CTTCAGAC TGATTGTTGTACCTGA; P2, CATCTGCTGCTCTTAGAG GAACA; P3, ACCTCTCTAGCCTCAGGAATGA; P4, TGATT CCCACTTTGTGGTTCTAAG. The mice were maintained in the modern animal housing facilities of the Turku Animal Centre under the guidelines of the University Ethics Committee.

### TISSUE SAMPLES

Mice were sacrificed at the age of 8 weeks. Body and spleen weights were measured. Tissue samples including liver, spleen, kidneys, heart, skeletal muscle, central nervous system, reproductive organs,

digestive track, femur, tibia, and calvaria were collected and fixed with 10% formalin for 24–48 h. For the paraffin embedding, the tibias and femurs were decalcified with 10% EDTA incubation for 2 weeks.

### HISTOLOGICAL ANALYSIS

Sections, 7.5 μm thick, of tibia bone and other tissue slices were cut on SuperFrost Plus microscope slides (Menzel-Gläser; Braunschweig, Germany), and stained with hematoxylin and eosin (HE), and Elastica van Gieson. Histochemical staining for tartrate resistant acid phosphatase (TRACP) (Acid Phosphatase Leukocyte (Trap) Kit, Sigma–Aldrich, Steinheim, Germany) was used to visualize osteoclasts under light microscopy. The staining was carried out according to manufacturer's instructions, and sections were counterstained with Mayer's hematoxylin. Tibia and spleen sections were immunolabeled with avidin–biotin method. The sections were deparaffinized, and hydrated in a descending ethanol series. For antigen retrieval, the sections were boiled in 10 mM citrate buffer pH 6.0 for 15 min. Endogenous peroxidase activity was quenched by treating the sections in 0.3% $H_2O_2$ for 30 min. To prevent non-specific binding, the sections were incubated in horse serum diluted in PBS. Primary antibodies for Phospho-p44/42 MAP Kinase (Thr202/Tyr204) and p44/42 MAP Kinase (both from Cell Signaling Technology, Beverly, MA) were diluted in 1% BSA-PBS and incubated on the samples overnight at 4°C. The bound antibodies were visualized using appropriate avidin–biotin peroxidase kit (Vectastain; Vector Laboratories, Burlingame, CA) with 3,3′-diaminobenzidine tetrahydrochloride (DAB) as the chromogen (DAB peroxidase substrate kit; Vector Laboratories). Sections were counterstained with Mayer's hematoxylin (Reagena LTD; Kuopio, Finland). In negative control reactions primary antibody was replaced with 1% BSA-PBS.

### MICROSCOPY AND HISTOMORPHOMETRIC ANALYSIS OF SPLEEN

Histological sections were imaged by Olympus BX51TF Digital Virtual Microscope (Olympus, Tokyo, Japan) in vsi file format, and analyzed by dotSlide software (Soft Imaging System GmbH, Münster, Germany). For histomorphometric analysis of spleen with dotSlide software, four equal areas ($1 \times 10^6$ μm$^2$) from each HE stained sections were randomly selected and areas of white and red pulp were measured. Percentage of white pulp compared to total tissue area was calculated, and the number of megakaryocytes (MKs) and their total area were determined from the histological sections.

### OSTEOCLAST CULTURE

The osteoclast precursors were isolated from spleen of $Nf1^{-/-}_{Ocl}$ and $Nf1^{+/+}_{Ocl}$ as described [Bradley and Oursler, 2008]. The cells were pressed out from spleen to culture MEM Alpha medium (GIBCO, Paisley, UK). Triplicate cultures of five million cells were plated onto 50 mm petri dish for Western blot and for DNA analysis. For bone resorption assays and IIF, 24 million cells were plated to bovine bone slice in 24-well plate. Five mice ($n = 5$) from each genotype were used and five parallel cultures/mouse were established. The cells were differentiated into osteoclasts in the presence of RANKL (20 ng/ml, Peprotech, Rocky Hill, NJ) and M-CSF (10 ng/ml, R&D systems, Minneapolis, MN). DNA was isolated with DNeasy® Blood & Tissue Kit (Qiagen) on days 0, 2, and 4. The PCR was performed to analyze the flox and recombinated alleles as described above.

### INDIRECT IMMUNOFLUORESCENCE LABELING

Bone slices were fixed with 4% paraformaldehyde in PBS for 20 min. Cells were then permeabilized using 0.1% Triton X-100 in PBS on ice for 5 min. To prevent non-specific binding, the bone slices were preincubated in 1% BSA-PBS for 30 min. The samples were labeled for antibodes Alexa Fluor 488® Phalloidin (Invitrogen, Grand Island, NY) and Hoechst 33342 nuclear stain (Invitrogen) diluted in 1% BSA-PBS and incubated for 1 h, at 20°C. The labeled samples were washed in PBS and mounted with Immu-Mount™ (Thermo Scientific, Loughborough, UK).

### BONE RESORPTION CAPACITY IN VITRO

Bone resorption was analyzed from culture media and bone slices. Culture medium was collected on 10th day and C-terminal telopeptide of type I collagen (CTX) concentration was measured using CrossLaps® for Culture (CTX-I) ELISA kit (Immunodiagnostic Systems Ltd., Boldon, Tyne and Wear, UK). Analysis was performed according to manufacturer's protocol and results were correlated to bone slice area. Resorption pits of bone slice were visualized by wheat germ agglutinin (WGA)-lectin labeling as described previously (Heervä et al., 2010).

### WESTERN BLOT

Osteoclast cultures were harvested on days 0, 2, and 4 in buffer containing 2% sodium dodecyl sulfate, 50 mM dithiothreitol, and 10 mM Tris, pH 6.8. Equal volumes (30 μl) of cell lysate were subjected to sodium dodecyl sulfate polyacrylamide gel electrophoresis in 10% gel. The proteins were then transfered to polyvinylidene difluoride Amersham Hybond-ECL membrane (Amersham Life Sciences, Little Chalfont, England) and processed for immunoblotting. Membranes were first blocked with 5% milk in TBS + 0.1% Tween-20 and immunolabeled using primary antibodies Phospho-p44/42 MAP Kinase (Thr202/Tyr204; Cell Signaling Technology), p44/42 MAP Kinase (Cell Signaling Technology) Phospho-AKT (ser473; Cell Signaling Technology), Rabbit polyclonal pan-AKT (phospho T308; Abcam, Cambridge, UK), Rabbit polyclonal pan-AKT (Abcam), and Akt1 (C-20) (Santa Cruz). Antibody for beta actin was used as a loading control. Swine-Anti-Rabbit Immunoglobulins/HRP (DAKO) and Rabbit-Anti-Goat Immunoglobulins/HRP (DAKO) were used as secondary antibodies and detected with enhanced chemiluminescence (ECL) (Amersham Life Sciences). Densitometry was analyzed with ImageJ software.

### ALIZARIN RED AND ALCIAN BLUE STAINING OF MICE

The skin, muscles, and internal organs were removed and the skeletons were fixed in 96% ethanol for 5 days. Mice were then stained with 0.015% alizarin red in 2% KOH for 8 h and 0.05% alcian blue in 80% ethanol and 20% acetic acid for 24 h. After staining, mouse samples were transferred to 2% KOH until their soft tissues were cleaned in a series of graded glycerin, and stocked in 100% glycerin [McLeod, 1980; Hogan et al., 1994].

### MICROCOMPUTER TOMOGRAPHY (CT) ANALYSIS

Formalin fixed tibias of $Nf1_{Ocl}^{+/+}$, $Nf1_{Ocl}^{+/-}$, and $Nf1_{Ocl}^{-/-}$ mice were scanned using a SkyScan 1072 (Skyscan, Aartselaar, Belgium) X-ray microtomograph with X-ray tube settings of 72 kV and 138 μA. Four hundred projections were scanned at pixel size of 5.32 μm with 1.3 s exposure time and 180° rotation using 0.45° rotation steps. Transmission X-ray images were recorded and primary data was reconstructed by NRecon 1.6.3.1 software (Skyscan). Trabecular and cortical bone analysis and visualization and bone mineral density (BMD) analysis were carried out by CTAn 1.9.3.0 and CTVol 2.1.1.0 softwares (Skyscan) according to manufacturer's guide. Thickness of growth plate was analyzed by DataViewer 1.4.2 software (Skyscan). Triplicate measurements were analyzed from the lateral, medial, and center parts of the growth plate.

### MICRODISSECTION ANALYSIS

Inactivation of the Nf1 gene was evaluated by using P.A.L.M. laser microdissection (ZEISS, Jena, Germany) of tissue sections followed by PCR genotyping. Paraffin embedded sections of tibia were stained with Trap-kit according to manufacturer. TRACP-positive osteoclasts, chondrocytes of growth plate and diaphyseal osteocytes were microdissected and samples of each cell type were pooled. DNA was isolated by using QIAamp DNA FFPE Tissue Kit (Qiagen) and PCR was performed in two parts. DNA was pre-amplified using the P1–P2 primers and program: denaturation at 98°C for 1 min; 25 cycles with denaturation at 98°C for 10 s; annealing at 62°C for 10 s; and extension at 72°C for 20 s; and followed by 72°C for 5 min. Pre-amplified DNA was treated as genomic DNA as described above (Genotyping).

### THREE-POINT BENDING ASSAY

The three-point bending assay was performed as previously described [Peng et al., 1994]. Tibial bones were compressed at a constant rate of 0.155 mm/s until breakdown. Mechanical parameters such as ultimate strength (maximal load in N) and energy absorbed by the bone tissue representing structural toughness were analyzed using RatBone analyzer v1.2 software (Timo Rautiala, Oulu, Finland).

### STATISTICAL ANALYSIS

The three-point bending, μCT, bone mineral density, ELISA assays, and histomorphometric analyses were evaluated by PASW Statistics 18 (SPSS Inc., Chicago, IL) software. The statistical data were tested for normality with Shapiro–Wilk analysis. According to normality, the statistical significance was evaluated with a one-way ANOVA (Tukey's test) or with a Kruskal–Wallis. $P < 0.05$ was considered to be a statistically significant value.

## RESULTS

### $Nf1_{Ocl}$ MICE

Nf1 flox/flox mice and TRAP-Cre mice were mated to create the $Nf1_{Ocl}$ mouse strain. Regardless of the osteoclast genotype, $Nf1_{Ocl}^{+/+}$, $Nf1_{Ocl}^{+/-}$, or $Nf1_{Ocl}^{-/-}$, the mice were apparently normal having similar body weight, stature, macroscopic skeleton, and cartilages as shown with alizarin red/alcian blue staining (Fig. 1). Internal organs of the mice were first evaluated macroscopically and then microscopically from tissue sections. The spleen weight of $Nf1_{Ocl}^{-/-}$ mice was almost 50% higher compared to the spleen weight of controls. No abnormalities were detected in other organs evaluated, including liver, kidneys, heart, skeletal muscle, central nervous system, bone marrow, reproductive organs, and digestive track.

### INACTIVATION OF THE Nf1 GENE IN BONE

A 280-bp PCR-fragment, representative of inactivated Nf1 gene, was detected only in osteoclast samples containing osteoclasts of the $Nf1_{Ocl}$ mice. A 350-bp PCR fragment representative of an intact Nf1 flox site was detected in all other tissue samples (Fig. 2). Thus, these results indicate that the inactivation of the Nf1 gene was successfully targeted to osteoclasts in bone. PCR analysis of spleen-derived cell cultures containing a subpopulation of osteoclast precursors revealed the presence of an intact Nf1 flox site. The 280-bp PCR-fragment, representative of inactivated Nf1 flox allele, was observed in $Nf1_{Ocl}^{-/-}$ cultures (Fig. 2D). Recombination was also seen in ear marks due to the circulating myeloid cells (data not shown).

### Ras IN Nf1-DEFICIENT OSTEOCLASTS

Ras activation was examined in tibial bones in by immunolabeling of tibial bone sections with antibody to phosphorylated p44/42. Positive labeling for phosphorylated p44/42 indicating Ras activation was localized to osteoclasts with $Nf1_{Ocl}^{-/-}$ genotype, while the control tibia sections were negative (Fig. 3A,B). The tibial sections of $Nf1_{Ocl}^{+/-}$ mice also displayed a positive immunoreaction for phosphorylated p44/42 (data not shown).

In vitro, differentiating osteoclast cultures displayed moderate up-regulation of phosphorylated p44/42 as estimated by western transfer analysis (Fig. 3C). In general, analysis of Ras activation showed twofold increase in $Nf1^{-/-}$ osteoclast cultures on average. Particularly on day 4 of cultures, the $Nf1^{-/-}$ osteoclasts showed higher levels of phosphorylated p44/42 compared to controls (Fig. 3D). This is in analogy to findings describing activation of Ras pathway in various cell types [Kim et al., 1995; Sherman et al., 2000; Zhu et al., 2001; Elefteriou et al., 2006; Yang et al., 2006; Kolanczyk et al., 2007].

Activation of phosphoinositide 3-kinase (PI3K) pathway was also evaluated in differentiating osteoclast cultures by western transfer analysis using two different antibodies for total Akt and two different antibodies for p-Akt. The results revealed activation of Akt, but it did not follow the same timetable in all sample sets. In conclusion, the $Nf1^{-}/^{-}$ samples showed increased p-Akt levels compared to control cells but the results were not conclusive (data not shown).

### MORPHOMETRIC ANALYSIS OF TIBIAL BONES USING μCT

Macroscopic differences in tibial bones were not detected between $Nf1_{Ocl}^{+/+}$, $Nf1_{Ocl}^{+/-}$, and $Nf1_{Ocl}^{-/-}$ mice. Tibial bones of 58 mice representing $Nf1_{Ocl}^{+/+}$, $Nf1_{Ocl}^{+/-}$, and $Nf1_{Ocl}^{-/-}$ genotypes were scanned with μCT, and three-dimensional models were reconstructed (Fig. 4).

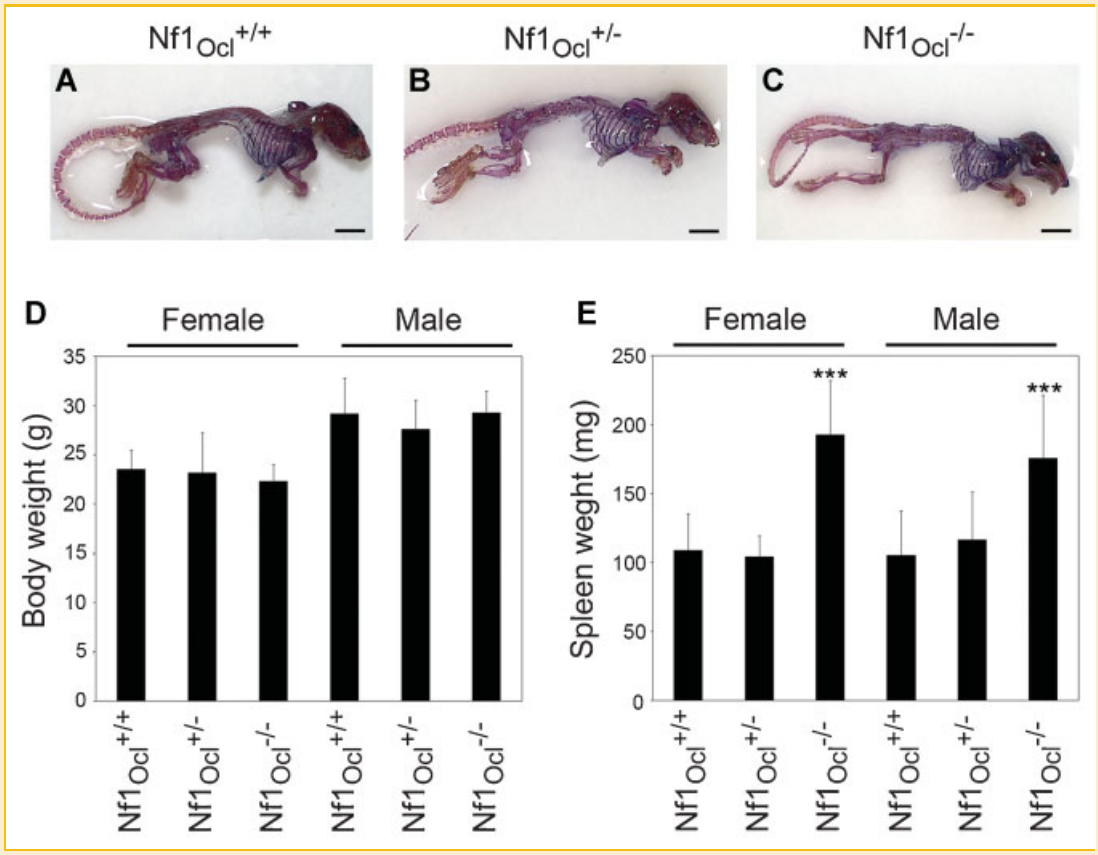


Fig. 1. Alizarin red/alcian blue stained 8-week-old mice harboring osteoclasts with $Nf1_{Ocl}^{+/+}$, $Nf1_{Ocl}^{+/-}$ and $Nf_{Ocl}^{-/-}$ genotypes (A–C). The red color indicates the mineralized bone and alcian blue shows the cartilage. Whole body weight (D) and spleen weight (E). The size of spleen in $Nf1_{Ocl}^{-/-}$ mice was enlarged compared to $Nf1_{Ocl}^{+/+}$ mice. $^{***}P < 0.001$, scale bar 1 cm.

Regions of interest were delineated in the diaphyseal and trabecular parts of tibia, and the reconstructed models were subjected to volumetric analysis [Parfitt et al., 1987].

Cortical bone was analyzed from the midshaft of tibia. The results showed that the perimeter and subsequently the cross-sectional area of tibial diaphysis were smaller in $Nf1_{Ocl}^{-/-}$ mice compared to controls (Table I). Regardless of genotype, the bone volume was equal, translating to relatively thicker cortical bone and narrower bone marrow cavity in $Nf1_{Ocl}^{-/-}$ mice. Measurements of four anatomically defined points showed that the cortical thickness was equally distributed into anterior, lateral, medial and posterior parts of diaphyseal bone.

The trabecular bone was analyzed from the proximal metaphysis of tibia. A smaller bone volume and a smaller number of trabecles were noted particularly in $Nf1_{Ocl}^{-/-}$ male mice. In general, the skeletal findings on $Nf1_{Ocl}^{+/-}$ mice fell between those of $Nf1_{Ocl}^{-/-}$ and controls (Table II).

Reconstructed μCT images of tibial bones were used to measure the thickness of growth plate at three different points. The results showed that the growth plate of $Nf1_{Ocl}^{-/-}$ mice was 20% narrower than in control mice (Fig. 4). Male and female mice displayed similar results. Histological analysis demonstrated that in particular the proliferative zone of the growth plate was less prominent compared to controls. Also, the chondrocytes in columns were less organized (Fig. 4D).

Bone mineral density analyses from trabecular and cortical bone revealed no alterations between $Nf1_{Ocl}^{-/-}$ mice and control mice (Tables I and II). Thus, osteopenic or osteoporotic bone phenotype could not be demonstrated. This is in accordance with the results of tibial three-point bending test which did not reveal differences in mechanical strength between $Nf1_{Ocl}^{+/+}$, $Nf1_{Ocl}^{+/-}$, and $Nf1_{Ocl}^{-/-}$ genotypes (data not shown).

## DIFFERENTIATION OF Nf1 DEFICIENT OSTEOCLASTS IN VITRO

In order to analyze spleen derived osteoclast cultures in more detail, the number of osteoclasts and actin ring formation were studied. Cells containing more than three nuclei were counted as mature osteoclasts. The results showed equal numbers of differentiated osteoclasts in both genotypes. The ratio of $Nf1_{Ocl}^{+/+}$ versus $Nf1_{Ocl}^{-/-}$ was 1:1.002, $P = 0.908$ (data not shown). The cytoskeleton was labeled with phalloidin and the analysis revealed highly variable actin ring formation in $Nf1_{Ocl}^{-/-}$ osteoclasts compared to $Nf1_{Ocl}^{+/+}$ osteoclasts (Fig. 5A,B). More specifically, the cell size was variable particularly in $Nf1_{Ocl}^{-/-}$ osteoclasts which occasionally contained several small actin rings (Fig. 5B).

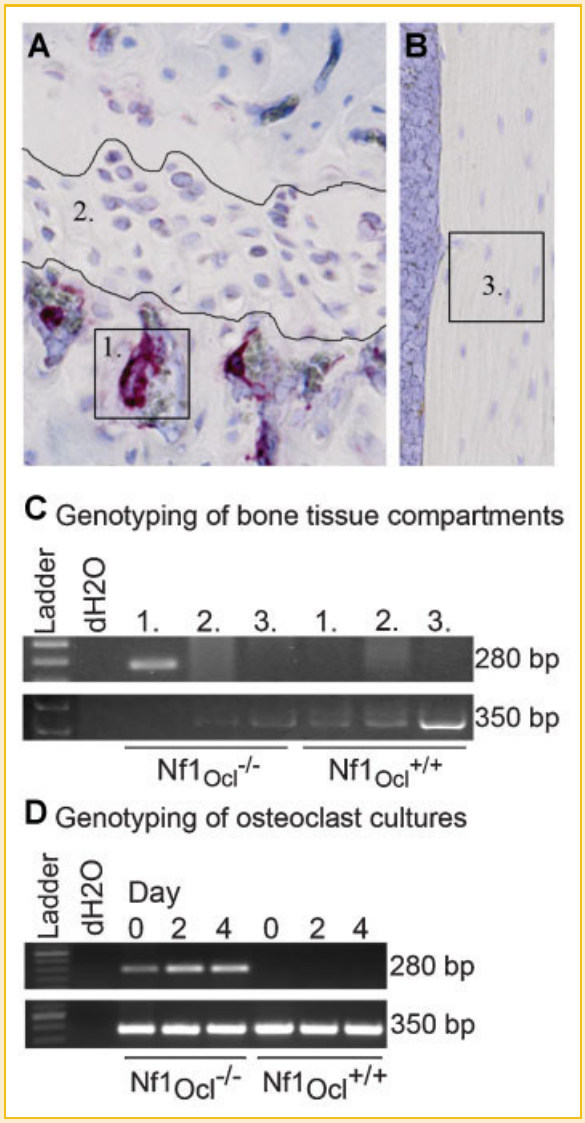


Fig. 2. TRACP staining of proximal tibia (A) shows TRACP positive osteoclasts (1.) close to the growth plate (2.), and hematoxylin counterstaining reveals nuclei of osteocytes (3.) in cortical bone (B). Tissue specimens for cell type specific genotyping were collected using laser microdissection. Genomic DNA was isolated from TRACP-positive osteoclasts (1. in A), the chondrocytes of growth plate (2. in A) and osteocytes of cortical bone (3. in B). PCR amplified a characteristic 280 bp band representative of recombination of the Nf1 allele in $Nf1^{-/-}_{Ocl}$ osteoclasts only (C). A 350 bp fragment representing an intact Nf1 flox site was amplified by PCR from the other DNA samples. PCR analysis of spleen-derived cell cultures containing a subpopulation of osteoclast precursors revealed the presence of an intact Nf1 flox site in $Nf1^{+/+}_{Ocl}$ and $Nf1^{-/-}_{Ocl}$ mice (D). The 280 bp PCR-fragment representative of inactivated Nf1 flox allele was observed in $Nf1^{-/-}_{Ocl}$ cultures on days 0, 2, and 4.

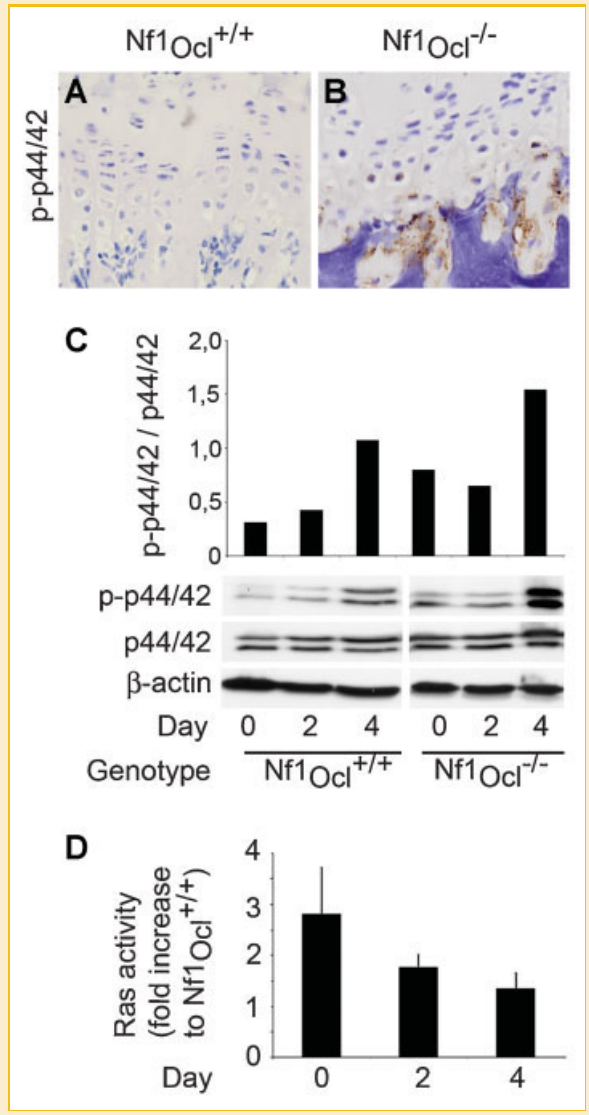


Fig. 3. Avidin–biotin immunolabeling for phosphorylated p44/42 in proximal tibia (A,B). The brown DAB color reaction indicates phosphorylated p44/42 positive osteoclasts in $Nf1^{-/-}_{Ocl}$ mice (B). Western blot analysis of osteoclast cultures for p44/42 and phosphorylated p44/42. The bars represent p-p44/42/p44/42 ratios (C). The bars represent relative increase of phosphorylated p44/42 in $Nf1^{-/-}$ osteoclasts compared to $Nf1^{+/+}$ osteoclasts (D).

## BONE RESORPTION CAPACITY OF Nf1Ocl MICE IN VITRO

The bone resorption capacity of osteoclasts was analyzed by measuring the type I collagen degradation product, CTX in culture media of osteoclasts on bone slide, and by visualing the resorption pits. The results showed significantly higher CTX concentrations (mean ± SEM; $Nf1^{-/-}_{Ocl}$ $0.096 \pm 0.006$ nM/mm$^2$ vs. $Nf1^{+/+}_{Ocl}$ $0.065 \pm 0.007$, $P < 0.002$) in medium collected from $Nf1^{-/-}_{Ocl}$ cultures compared to $Nf1^{+/+}_{Ocl}$ (Fig. 5E). WGA-lectin revealed more abundant and less organized resorption pits in bone slice of $Nf1^{-/-}_{Ocl}$ cultures compared to those of $Nf1^{+/+}_{Ocl}$ cultures (Fig. 5C,D). Analyses of CTX concentrations and bone resorption pits thus displayed corresponding results.

## HISTOMORPHOMETRIC ANALYSIS OF SPLEEN

The histological appearance of the spleen was normal despite the enlarged size. The ratios of red and white pulp areas were measured and the results were similar. Specifically, white pulp covered 40% of the total area in $Nf1^{-/-}_{Ocl}$ spleens and 42% in control spleens (Fig. 6).

TABLE I. MicroCT Analysis of Cortical Bone of Tibial Diaphysis

| Cortical bone | $Nf1^{+/+}_{Ocl}$ male (n = 11) | $Nf1^{+/-}_{Ocl}$ Male (n = 8) | $Nf1^{-/-}_{Ocl}$ Male (n = 8) | $Nf1^{+/+}_{Ocl}$ Female (n = 11) | $Nf1^{+/-}_{Ocl}$ Female (n = 14) | $Nf1_{Ocl}{}^{-/-}$ Female (n = 8) |
|---|---|---|---|---|---|---|
| Tissue volume ($mm^3$) | 0.487 ± 0.05 | 0.46 ± 0.04 | 0.43 ± 0.04* | 0.41 ± 0.03 | 0.41 ± 0.04 | 0.36 ± 0.03* |
| Bone volume ($mm^3$) | 0.265 ± 0.02 | 0.25 ± 0.02 | 0.25 ± 0.02 | 0.23 ± 0.02 | 0.23 ± 0.02 | 0.22 ± 0.02 |
| Mean total crossectional tissue area ($mm^2$) | 1.79 ± 0.18 | 1.68 ± 0.15 | 1.58 ± 0.162* | 1.52 ± 0.12 | 1.52 ± 0.13 | 1.32 ± 0.12* |
| Mean total crossectional tissue perimeter (mm) | 6.74 ± 0.43 | 6.80 ± 0.35 | 6.75 ± 0.49 | 6.36 ± 0.30 | 6.31 ± 0.31 | 5.83 ± 0.34* |
| BMD ($g/cm^3$) | 633.6 ± 56.68 | 614 ± 65.74 | 632.61 ± 71.00 | 627.68 ± 42.50 | 663.98 ± 104.86 | 688.64 ± 60.11 |

*Compared to $Nf1^{+/+}_{Ocl}$, $P < 0.05$.

There was no evidence of increased myeloid cell proliferation. However, the number of splenic megakaryocytes was greatly increased in $Nf1^{-/-}_{Ocl}$ (8.5 MKs/$mm^2$) compared to control mice (3.2 MKs/$mm^2$, $P < 0.0001$).

## DISCUSSION

The $Nf1_{Ocl}$ mouse model was generated to further elucidate the role of Nf1-deficiency in osteoclasts. The results of the present study show that inactivation of the Nf1 gene was successfully targeted to osteoclasts in bone in $Nf1^{-/-}_{Ocl}$ mice. This is in accordance with the findings by Dossa et al. who, by using the same TRACP promoter, described specific inactivation of intergrin-linked kinase in osteoclasts [Dossa et al., 2010]. The $Nf1_{Ocl}$ mouse model demonstrated mild but specific features in bone with no evidence of osteoporosis. Specifically, mechanical strength or bone mineral density did not differ between the $Nf1^{-/-}_{Ocl}$ and control mice. These findings suggest that Nf1 deficiency in osteoclasts alone is not sufficient to promote the osteoporotic bone phenotype. μCT revealed tibias with smaller perimeter and reduced diameter of bone marrow cavity in $Nf1^{-/-}_{Ocl}$ mice. Similar results have been reported on patients with NF1 where CT analysis showed localized changes in the distal part of tibia: bone was thinner, bone marrow cavity was smaller and bone mineral density was decreased compared to healthy controls even though the NF1 patients did not have any clinically detectable skeletal abnormalities [Stevenson et al., 2009].

Despite the fact that there was no evidence of Nf1 gene inactivation or Ras activation in chondrocytes, alterations in the growth plate were noted in $Nf1^{-/-}_{Ocl}$ mice. Specifically, narrowed growth plate and less well-organized chondrocytes in columns were detected in the proximal tibia in $Nf1^{-/-}_{Ocl}$ mice compared to control mice. Previous studies have shown that inactivation of the Nf1 gene in mesenchymal stem cells and mature chondrocytes leads to the narrowed growth plate and the activation of Ras pathway in chondrocytes [Kolanczyk et al., 2007]. Ras activation has also been observed in normal chondrocytes during the bone healing and occasionally in hypertrophic chondrocytes in normal bone [Kuorilehto et al., 2004, 2006]. The current study revealed increased Ras pathway activation in $Nf1^{-/-}$ osteoclasts in vivo and in vitro. Previous study [Yang et al., 2006] and our results suggest that Ras and Akt pathways are independently regulated in osteoclasts. A recent study has also revealed hyperactivated mTOR pathway in abnormal osteoclastogenesis in Nf1-deficient mice [Ma et al., 2012]. These findings collectively suggest that Nf1-deficiency in osteoclasts leads to alterations in cell signaling at multiple levels. We speculate that Nf1 deficient osteoclasts may have an influence also on the chondrocytes of $Nf1_{Ocl}$ mice.

Most of the bone-related Nf1-deficient mouse models have revealed mild skeletal abnormalities in vivo. Instead, findings in vitro revealed several significant defects under conditions free from factors operative in live animals. The current study also showed increased bone resorption capacity and abnormal cell shape, and actin ring formation. Increased bone resorption may be related to osteopenia/osteoporosis seen in NF1 patients.

Our study revealed an unexpected result that $Nf1^{-/-}_{Ocl}$ mice had enlarged spleen compared to control mice even though the body weight was similar in each genotype. Histomorphometric analysis showed that the ratio between the red and the white pulp was similar in each genotype even though the weight and size of spleen were markedly increased in $Nf1^{-/-}_{Ocl}$ mice. Also an increased number of megakaryocytes was detected in $Nf1^{-/-}_{Ocl}$ spleens. Even though TRACP is expressed in mouse spleen, we could not find any evidence of MKs expressing TRACP in spleen or in bone marrow in $Nf1^{-/-}_{Ocl}$

TABLE II. MicroCT Analysis of Trabecular Bone of Proximal Tibia

| Trabecular bone | $Nf1^{+/+}_{Ocl}$ Male | $Nf1^{+/-}_{Ocl}$ Male | $Nf1^{-/-}_{Ocl}$ Male | $Nf1^{+/+}_{Ocl}$ Female | $Nf1^{+/-}_{Ocl}$ Female | $Nf1_{Ocl}{}^{-/-}$ Female |
|---|---|---|---|---|---|---|
| Tissue volume ($mm^3$) | 3.64 ± 0.44 | 3.60 ± 0.41 | 3.08 ± 0.34* | 2.71 ± 0.29 | 2.58 ± 0.40 | 2.27 ± 0.37 |
| Bone volume ($mm^3$) | 0.65 ± 0.20 | 0.52 ± 0.09 | 0.47 ± 0.13* | 0.32 ± 0.08 | 0.34 ± 0.17 | 0.30 ± 0.08 |
| Trabecular thickness (mm) | 0.09 ± 0.01 | 0.11 ± 0.03 | 0.09 ± 0.01 | 0.08 ± 0.01 | 0.08 ± 0.01 | 0.08 ± 0.01 |
| Trabecular number (1/mm) | 2.03 ± 0.44 | 1.45 ± 0.29* | 1.65 ± 0.30** | 1.41 ± 0.31 | 1.57 ± 0.58 | 1.63 ± 0.40 |
| Trabecular separation (mm) | 0.22 ± 0.06 | 0.17 ± 0.07 | 0.19 ± 0.06 | 0.26 ± 0.05 | 0.24 ± 0.07 | 0.19 ± 0.06* |
| BMD ($g/cm^3$) | 201.32 ± 45.85 | 173 ± 23.41 | 165.08 ± 32.56 | 145.13 ± 17.14 | 138 ± 29.16 | 158.46 ± 28.74 |

*Compared to $Nf1^{+/+}_{Ocl}$.
**Compared to $Nf1^{+/-}_{Ocl}$, $P < 0.05$.

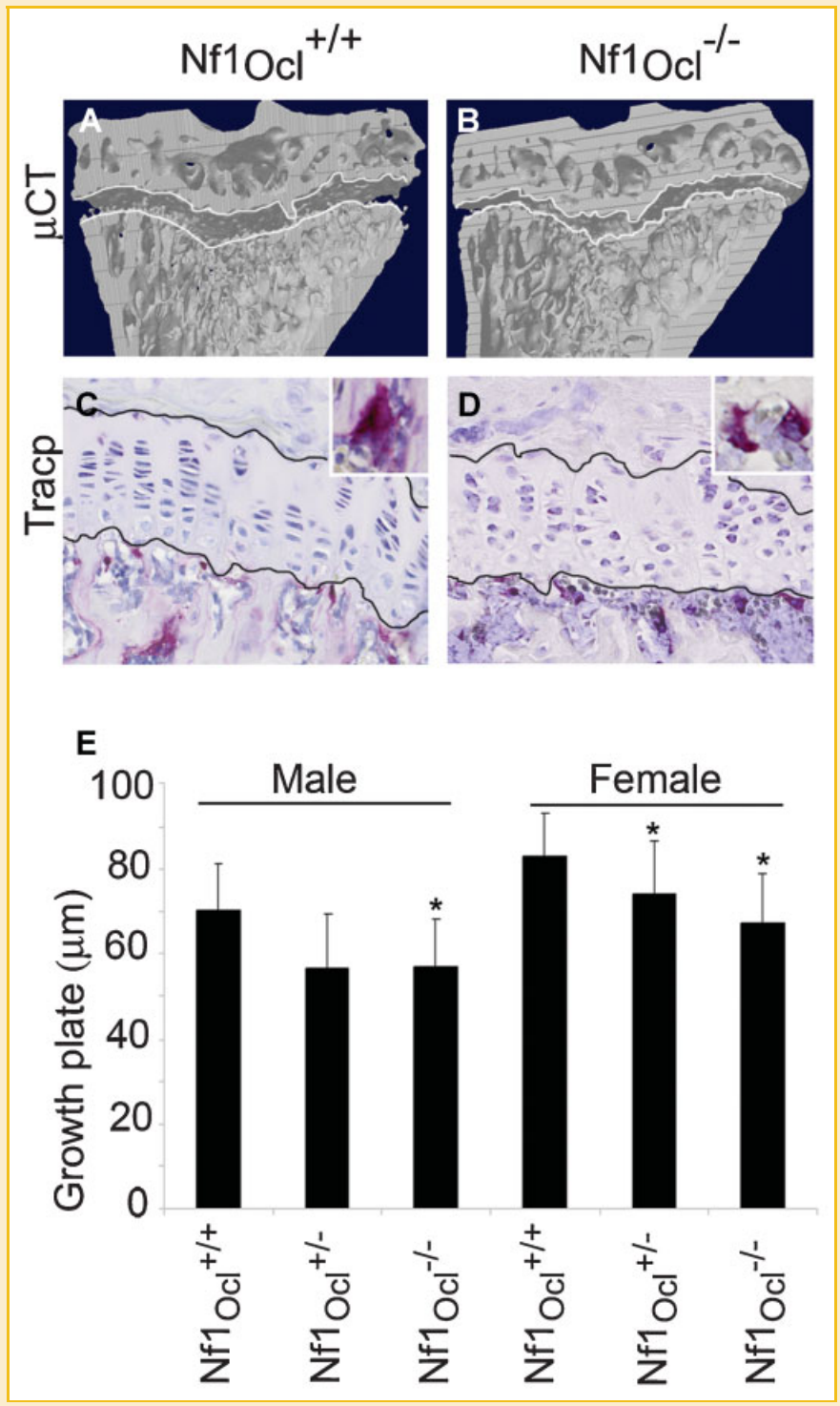


Fig. 4. µCT images (A,B) and TRACP staining (C,D) of growth plate of $Nf1_{Ocl}^{+/+}$ and $Nf1_{Ocl}^{-/-}$ mice. Sections of proximal tibia show the proliferative and hypertrophic zones in growth plate and osteoclasts in purple (C,D). Thickness of growth plate was measured from three different points using the DataViewer software (E). $^{*}P < 0.05$.

mice. The results suggest that bone phenotype, splenomegaly, and splenic megakaryocytosis in $Nf1_{Ocl}^{-/-}$ mice resulted from the Nf1 deficiency.

Previously, splenomegaly has been reported in Mx1, $Nf1^{flox/flox}$ mouse strain where Nf1 gene inactivation has been targeted to hematopoietic cells. The results showed progressive splenomegaly, expansion of red pulp with myeloid infiltration, but not splenic megakaryocytosis, megakaryocytosis, or thrombocytosis [Le et al., 2004]. Interestingly, thrombocytosis has been reported in a patient with NF1 [Hasle et al., 1997].

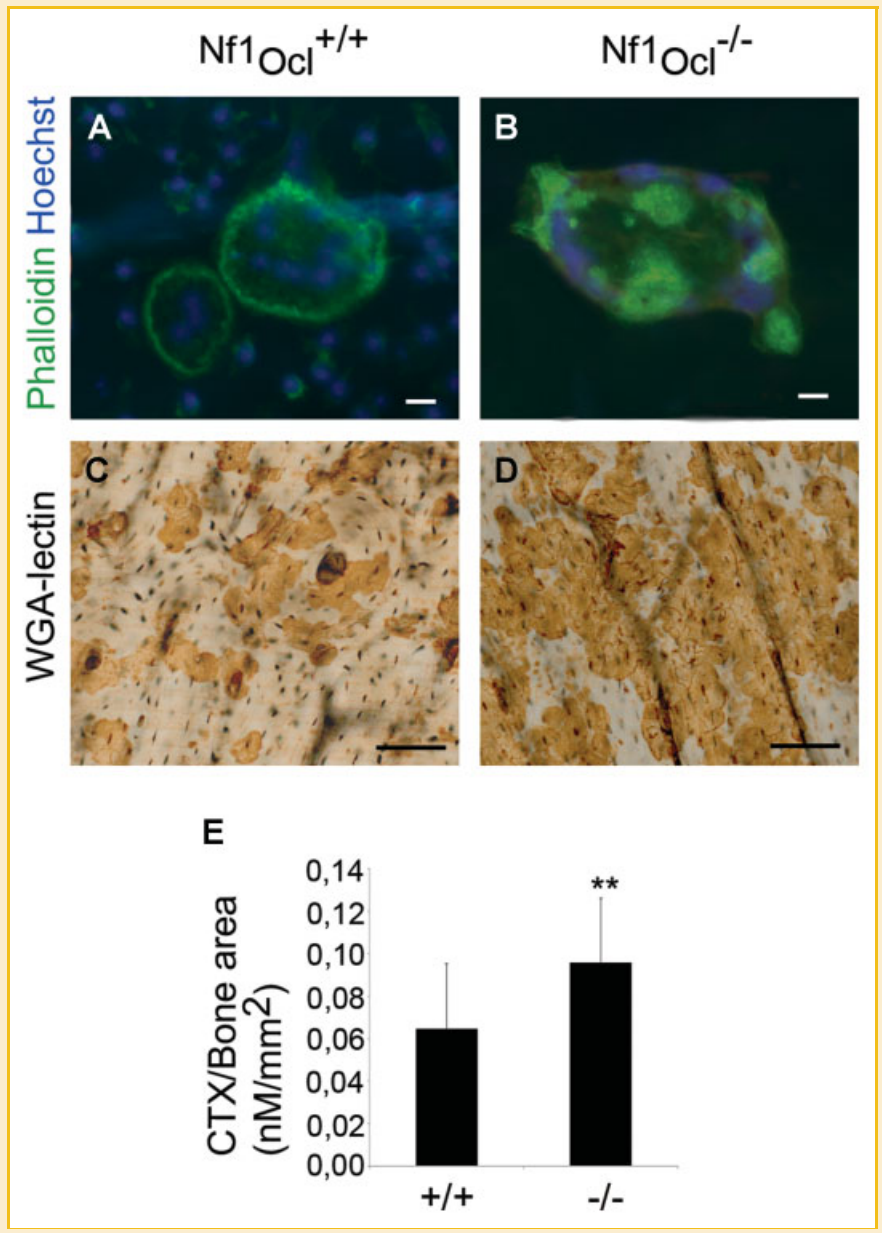


Fig. 5. $Nf1^{+/+}_{Ocl}$ and $Nf1^{-/-}_{Ocl}$ osteoclasts in vitro. Phalloidin fluorescence demonstrates f-actin in $Nf1^{+/+}_{Ocl}$ and $Nf1^{-/-}_{Ocl}$ osteoclasts (A,B), scale bar 10 μm. WGA-lectin staining visualizes resorption pits in bone slices (C,D), scale bar 100 μm. The CTX concentrations of culture media were adjusted to bone slice areas in $Nf1^{-/-}_{Ocl}$ and $Nf1^{+/+}_{Ocl}$ cultures (E). $^{**}P < 0.01$. [Color figure can be seen in the online version of this article, available at http://wileyonlinelibrary.com/journal/jcb]

Osteoclastogenesis is regulated by osteoblasts through RANKL, OPG, and M-CSF [Rodan and Martin, 1981; Biskobing et al., 1995; Simonet et al., 1997]. It is of interest to note that MKs also participate in bone homeostasis and remodeling by synthesizing OPG and RANKL [Bord et al., 2004, 2005]. It has earlier been shown that megakaryocytosis leads to osteosclerotic bone phenotype with enhanced osteoblast formation and inhibition of osteoclastogenesis and bone resorption [Villeval et al., 1997; Garimella et al., 2007; Suva et al., 2008]. Our Nf1-deficient osteoclast mouse model displayed mild bone phenotype although the original hypothesis was that inactivation of Nf1 gene in osteoclasts would lead to osteopenic/osteoporotic bone. We speculate that splenomegaly and the high number of splenic MKs might participate in bone homeostasis by limiting osteoclastogenesis and bone resorption in vivo.

We generated a mouse model where the inactivation of Nf1 gene was successfully targeted to osteoclasts. Summarizing the results, $Nf1^{-/-}_{Ocl}$ mouse produced a mild but specific bone phenotype including changes in trabecular and cortical bone, as well as in non-mineralized tissues such as narrowed growth plate, splenomegaly and splenic megakaryocytosis. Furthermore, $Nf1^{-/-}$ osteoclasts had higher resorption capacity and abnormal actin ring formation in vitro. This study shows that NF1-deficiency in osteoclasts plays a role in the development of NF1-related skeletal abnormalities, but Nf1-deficiency in osteoclasts in $Nf1^{+/+}$ background is not sufficient

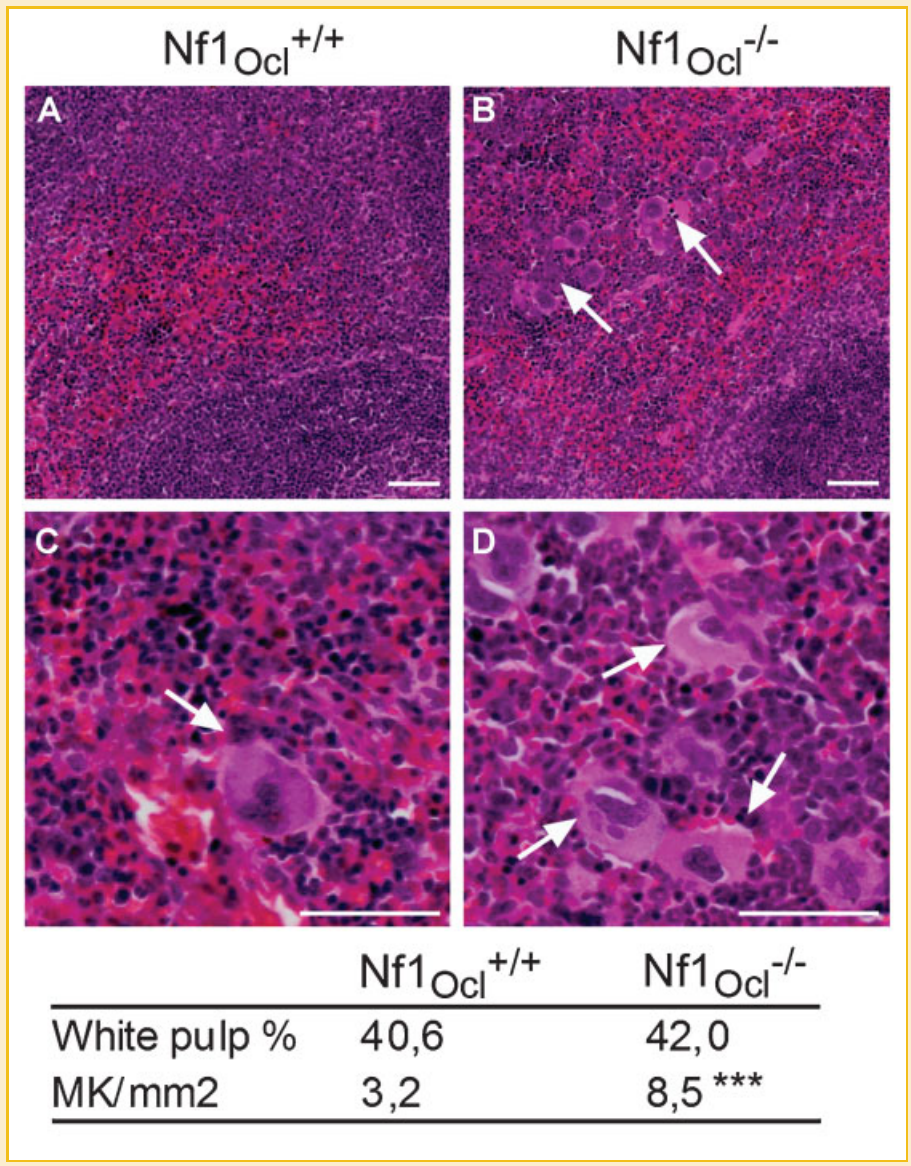


Fig. 6. H&E stained spleen of $Nf1_{Ocl}^{+/+}$ and $Nf1_{Ocl}^{-/-}$ mice showing red and white pulp (A–D). Arrows indicate megakaryocytes in white pulp. Histomorphometric analysis of spleens in $Nf1_{Ocl}^{-/-}$ and $Nf1_{Ocl}^{+/+}$ mice including percentage of white pulp and number of MKs/mm$^2$ were analyzed with dotSlide software. $^{***}P < 0.001$, scale bar 50 μm. [Color figure can be seen in the online version of this article, available at http://wileyonlinelibrary.com/journal/jcb]

to induce skeletal abnormalities analogous to those observed in patients with NF1, even though the $Nf1^{-/-}$ osteoclasts display increased resorption capacity in vitro.

## ACKNOWLEDGMENTS

This work was supported by Academy of Finland (JP). M.H.A. is a recipient of the National Graduate School of Clinical Investigation, Finland.

## REFERENCES

Biskobing DM, Fan X, Rubin J. 1995. Characterization of MCSF-induced proliferation and subsequent osteoclast formation in murine marrow culture. J Bone Miner Res 10:1025–1032.

Bord S, Frith E, Ireland DC, Scott MA, Craig JI, Compston JE. 2004. Synthesis of osteoprotegerin and RANKL by megakaryocytes is modulated by oestrogen. Br J Haematol 126:244–251.

Bord S, Frith E, Ireland DC, Scott MA, Craig JI, Compston JE. 2005. Megakaryocytes modulate osteoblast synthesis of type-l collagen, osteoprotegerin, and RANKL. Bone 36:812–819.

Bradley E, Oursler M. 2008. Osteoclast culture and resorption assays. Methods Mol Biol 455:19–35.

Brannan C, Perkins A, Vogel K, Ratner N, Nordlund M, Reid S, Buchberg A, Jenkins N, Parada L, Copeland N. 1994. Targeted disruption of the neurofibromatosis type-1 gene leads to developmental abnormalities in heart and various neural crest-derived tissues. Genes Dev 8:1019–1029.

Buchberg AM, Cleveland LS, Jenkins NA, Copeland NG. 1990. Sequence homology shared by neurofibromatosis type-1 gene and IRA-1 and IRA-2 negative regulators of the RAS cyclic AMP pathway. Nature 347:291–294.

Dossa T, Arabian A, Windle JJ, Dedhar S, Teitelbaum SL, Ross FP, Roodman GD, St-Arnaud R. 2010. Osteoclast-specific inactivation of the integrin-linked kinase (ILK) inhibits bone resorption. J Cell Biochem 110:960–967.

Elefteriou F, Benson M, Sowa H, Starbuck M, Liu X, Ron D, Parada L, Karsenty G. 2006. ATF4 mediation of NF1 functions in osteoblast reveals a nutritional basis for congenital skeletal dysplasiae. Cell Metab 4:441–451.

Elefteriou F, Kolanczyk M, Schindeler A, Viskochil D, Hock J, Schorry E, Crawford A, Friedman J, Little D, Peltonen J, Carey J, Feldman D, Yu X, Armstrong L, Birch P, Kendler D, Mundlos S, Yang F, Agiostratidou G, Hunter-Schaedle K, Stevenson D. 2009. Skeletal abnormalities in neurofibromatosis type 1: Approaches to therapeutic options. Am J Med Genet A 149A:2327–2338.

Feng X. 2005. RANKing intracellular signaling in osteoclasts. IUBMB Life 57:389–395.

Garimella R, Kacena MA, Tague SE, Wang J, Horowitz MC, Anderson HC. 2007. Expression of bone morphogenetic proteins and their receptors in the bone marrow megakaryocytes of GATA-1(low) mice: A possible role in osteosclerosis. J Histochem Cytochem 55:745–752.

Hasle H, Nir M, Tommerup N. 1997. Prolonged extreme thrombocytosis associated with neurofibromatosis type 1. J Pediatr 130:317–319.

Heervä E, Alanne M, Peltonen S, Kuorilehto T, Hentunen T, Väänänen K, Peltonen J. 2010. Osteoclasts in neurofibromatosis type 1 display enhanced resorption capacity, aberrant morphology, and resistance to serum deprivation. Bone 47:583–590.

Hogan B, Beddington R, Constatini F, Lacy E. 1994. Techniques for visualizing gene products, cells, tissues, and organ systems. In: Nagy A, Gertsenstein M, Vintersten K, Behringer R, editors. Manipulating the mouse embryo: A laboratory manual. Woodbury, NY: Cold Spring Harbor Laboratory Press. pp. 699–701.

Jacks T, Shih T, Schmitt E, Bronson R, Bernards A, Weinberg R. 1994. Tumour predisposition in mice heterozygous for a targeted mutation in Nf1. Nat Genet 7:353–361.

Jouhilahti EM, Peltonen S, Heape AM, Peltonen J. 2011. The pathoetiology of neurofibromatosis 1. Am J Pathol 178:1932–1939.

Kim H, Rosenbaum T, Marchionni M, Ratner N, DeClue J. 1995. Schwann cells from neurofibromin deficient mice exhibit activation of p21ras, inhibition of cell proliferation and morphological changes. Oncogene 11:325–335.

Kolanczyk M, Kossler N, Kühnisch J, Lavitas L, Stricker S, Wilkening U, Manjubala I, Fratzl P, Spörle R, Herrmann B, Parada L, Kornak U, Mundlos S. 2007. Multiple roles for neurofibromin in skeletal development and growth. Hum Mol Genet 16:874–886.

Kossler N, Stricker S, Rödelsperger C, Robinson PN, Kim J, Dietrich C, Osswald M, Kühnisch J, Stevenson DA, Braun T, Mundlos S, Kolanczyk M. 2011. Neurofibromin (Nf1) is required for skeletal muscle development. Hum Mol Genet 14:2697–2709.

Kuorilehto T, Nissinen M, Koivunen J, Benson M, Peltonen J. 2004. NF1 tumor suppressor protein and mRNA in skeletal tissues of developing and adult normal mouse and NF1-deficient embryos. J Bone Miner Res 19:983–989.

Kuorilehto T, Ekholm E, Nissinen M, Hietaniemi K, Hiltunen A, Paavolainen P, Penttinen R, Peltonen J. 2006. NF1 gene expression in mouse fracture healing and in experimental rat pseudarthrosis. J Histochem Cytochem 54:363–370.

Le DT, Kong N, Zhu Y, Lauchle JO, Aiyigari A, Braun BS, Wang E, Kogan SC, Le Beau MM, Parada L, Shannon KM. 2004. Somatic inactivation of Nf1 in hematopoietic cells results in a progressive myeloproliferative disorder. Blood 103:4243–4250.

Leskelä H, Kuorilehto T, Risteli J, Koivunen J, Nissinen M, Peltonen S, Kinnunen P, Messiaen L, Lehenkari P, Peltonen J. 2009. Congenital pseudarthrosis of neurofibromatosis type 1: Impaired osteoblast differentiation and function and altered NF1 gene expression. Bone 44:243–250.

Ma J, Li M, Hock J, Yu X. 2012. Hyperactivation of mTOR critically regulates abnormal osteoclastogenesis in neurofibromatosis Type 1. J Orthop Res 30: 144–152.

McLeod M. 1980. Differential staining of cartilage and bone in whole mouse fetuses by alcian blue and alizarin red S. Teratology 22:299–301.

Parfitt A, Drezner M, Glorieux F, Kanis J, Malluche H, Meunier P, Ott S, Recker R. 1987. Bone histomorphometry: Standardization of nomenclature, symbols, and units. Report of the ASBMR Histomorphometry Nomenclature Committee. J Bone Miner Res 2:595–610.

Peng Z, Tuukkanen J, Zhang H, Jämsä T, Väänänen HK. 1994. The mechanical strength of bone in different rat models of experimental osteoporosis. Bone 15:523–532.

Riccardi V, Eichner J. 1986. Neurofibromatosis: Phenotype, natural history and pathogenesis. Baltimore, MD: Johns Hopkins University Press.

Rodan GA, Martin TJ. 1981. Role of osteoblasts in hormonal control of bone resorption–a hypothesis. Calcif Tissue Int 33:349–351.

Sherman L, Atit R, Rosenbaum T, Cox A, Ratner N. 2000. Single cell Ras-GTP analysis reveals altered Ras activity in a subpopulation of neurofibroma Schwann cells but not fibroblasts. J Biol Chem 275:30740–30745.

Simonet WS, Lacey DL, Dunstan CR, Kelley M, Chang MS, Lüthy R, Nguyen HQ, Wooden S, Bennett L, Boone T, Shimamoto G, DeRose M, Elliott R, Colombero A, Tan HL, Trail G, Sullivan J, Davy E, Bucay N, Renshaw-Gegg L, Hughes TM, Hill D, Pattison W, Campbell P, Sander S, Van G, Tarpley J, Derby P, Lee R, Boyle WJ. 1997. Osteoprotegerin: A novel secreted protein involved in the regulation of bone density. Cell 89:309–319.

Stevenson D, Viskochil D, Carey J, Slater H, Murray M, Sheng X, D'Astous J, Hanson H, Schorry E, Moyer-Mileur L. 2009. Tibial geometry in individuals with neurofibromatosis type 1 without anterolateral bowing of the lower leg using peripheral quantitative computed tomography. Bone 44:585–589.

Suva LJ, Hartman E, Dilley JD, Russell S, Akel NS, Skinner RA, Hogue WR, Budde U, Varughese KI, Kanaji T, Ware J. 2008. Platelet dysfunction and a high bone mass phenotype in a murine model of platelet-type von Willebrand disease. Am J Pathol 172:430–439.

Villeval JL, Cohen-Solal K, Tulliez M, Giraudier S, Guichard J, Burstein SA, Cramer EM, Vainchenker W, Wendling F. 1997. High thrombopoietin production by hematopoietic cells induces a fatal myeloproliferative syndrome in mice. Blood 90:4369–4383.

Wang W, Nyman JS, Ono K, Stevenson DA, Yang X, Elefteriou F. 2011. Mice lacking Nf1 in osteochondroprogenitor cells display skeletal dysplasia similar to patients with neurofibromatosis type I. Hum Mol Genet 20:3910–3924.

Xu GF, O'Connell P, Viskochil D, Cawthon R, Robertson M, Culver M, Dunn D, Stevens J, Gesteland R, White R. 1990. The neurofibromatosis type 1 gene encodes a protein related to GAP. Cell 62:599–608.

Yang F, Chen S, Robling A, Yu X, Nebesio T, Yan J, Morgan T, Li X, Yuan J, Hock J, Ingram D, Clapp D. 2006. Hyperactivation of p21ras and PI3K cooperate to alter murine and human neurofibromatosis type 1-haploinsufficient osteoclast functions. J Clin Invest 116:2880–2891.

Yasuda H, Shima N, Nakagawa N, Yamaguchi K, Kinosaki M, Mochizuki S, Tomoyasu A, Yano K, Goto M, Murakami A, Tsuda E, Morinaga T, Higashio K, Udagawa N, Takahashi N, Suda T. 1998. Osteoclast differentiation factor is a ligand for osteoprotegerin/osteoclastogenesis-inhibitory factor and is identical to TRANCE/RANKL. Proc Natl Acad Sci USA 95:3597–3602.

Yu X, Chen S, Potter O, Murthy S, Li J, Pulcini J, Ohashi N, Winata T, Everett E, Ingram D, Clapp W, Hock J. 2005. Neurofibromin and its inactivation of Ras are prerequisites for osteoblast functioning. Bone 36:793–802.

Zhang W, Rhodes SD, Zhao L, He Y, Zhang Y, Shen Y, Yang D, Wu X, Li X, Yang X, Park SJ, Chen S, Turner C, Yang FC. 2011. Primary osteopathy of vertebrae in a neurofibromatosis type 1 murine model. Bone 48:1378–1387.

Zhu Y, Romero M, Ghosh P, Ye Z, Charnay P, Rushing E, Marth J, Parada L. 2001. Ablation of NF1 function in neurons induces abnormal development of cerebral cortex and reactive gliosis in the brain. Genes Dev 15:859–876.